Rev. 113, 982 (1959).
[5]L. G. Radosevich and W. S. Williams, Phys. Rev. 181, 1110 (1969).
[6]A. B. Pippard, Phil. Mag. 46, 1104 (1955).
[7]L. G. Radosevich and W. S. Williams, Phys. Rev. 188, 770 (1969).
[8]P. G. Klemens and L. Tewordt, Rev. Mod. Phys. 36, 118 (1964).
[9]H. J. Levinstein and J. E. Kunzler, Phys. Letters 20, 581 (1966).
[10]P. Townsend and J. Sutton, Phys. Rev. 128, 591 (1962).
[11]K. Komenou, T. Yamashita, and Y. Onodera, Phys. Letters 28A, 335 (1968).

PHYSICAL REVIEW B VOLUME 4, NUMBER 1 1 JULY 1971

Tunneling into Weakly Coupled Films of Tin and Aluminum in Proximity. II. From the Tin Side*

J. Vrba and S. B. Woods
Department of Physics, University of Alberta, Edmonton 7, Canada
(Received 1 March 1971)

Tunneling experiments have been performed into the tin side of aluminum-tin proximity sandwiches evaporated at room temperature onto an oxidized aluminum electrode B. The coupling between the aluminum and tin films in proximity was made weak by allowing slight oxidation of the tin to occur at the interface. Using the McMillan model of the proximity structure, values of the electron-transmission probability α at the interface may be derived from the experiments. The α value is related to the critical temperature of the sandwich and also to the positions of peaks in the McMillan density of states. These peaks are reflected in the tunneling currents when the electrode B is superconducting. Values of α derived from these two kinds of measurements are found to be consistent and, qualitatively, to vary as expected with the oxidation conditions. Although the calculated curves of tunneling conductance as a function of applied voltage, when B is superconducting, exhibit sharper structure than the experimental curves, they are otherwise in good agreement. In contrast to tunneling from the aluminum side of the proximity sandwich, the tunneling characteristics into the tin side, when B is in the normal state, are similar to those into a BCS superconductor. On the whole, the experimental results are in good agreement with the predictions of the McMillan model.

INTRODUCTION

In recent papers[1,2] tunneling experiments into the aluminum side of aluminum-tin proximity sandwiches, when the aluminum thickness d_N was less than the tin thickness d_S, were reported. The occurrence of double-peaked structure was correlated with the predictions of the McMillan[3] tunneling model of the proximity effect and substantial quantitative agreement was obtained.

In a continuation of this work, measurements of the tunneling currents into the tin side of aluminum-tin proximity sandwiches with $d_s < d_N$ have been performed. The electron coupling between the metals was made weak by allowing slight oxidation of the tin to occur before the aluminum was deposited. The electron-transmission probability α at the proximity interface may be crudely controlled with the oxidation conditions and is qualitatively similar to that obtained by oxidation of aluminum.[1] The tunnel characteristics from a normal-state metal look like those into a BCS superconductor and do not offer any information about the properties of the sandwich. This is in contrast to the situation when tunneling into the aluminum side of the sandwich. The tunneling currents between a superconductor and the tin side of the proximity sandwich, on the other hand, exhibit a double-peaked structure over a considerable range of tin thickness. Again, in this investigation the experimental results are compared with calculations based on the McMillan model.

CALCULATIONS FOR TIN-ALUMINUM SANDWICHES

All the equations necessary for computer calculations with the McMillan model are presented in Ref. 1. Here, we present graphically the results of calculations with the McMillan model when $d_N > d_S$. An analysis of the tunneling density of states in the tin film is given. Again, we refer to aluminum as the normal-state metal (even when it is superconducting) and tin as the superconductor.

The double-peaked density of states seen in the aluminum side also exists in the tin side of the sandwich when α is sufficiently small. The exact shape and energy position of the peaks depend on the parameters Γ_S, Γ_N, Δ_S^{ph}, and Δ_N^{ph}. The behavior is illustrated in Fig. 1 for three different values of

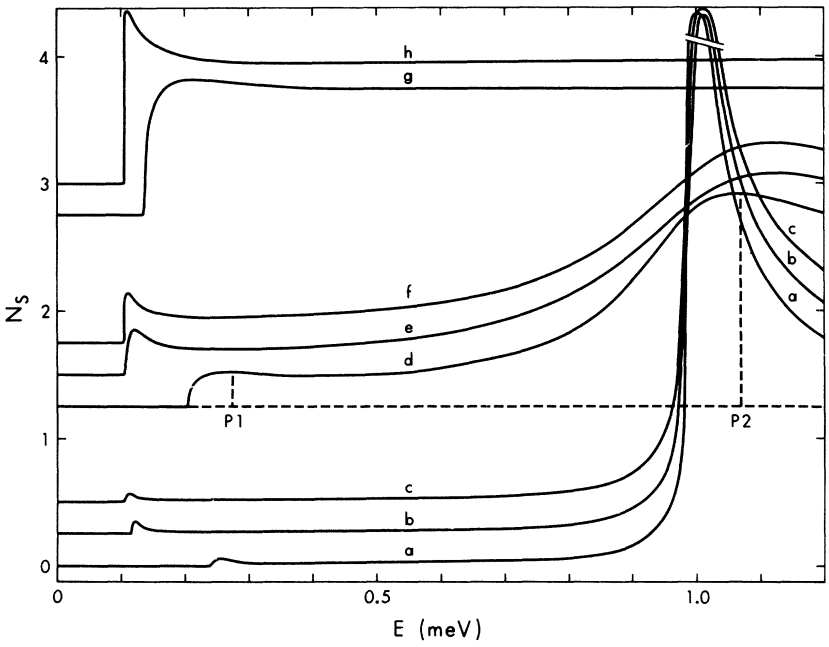

FIG. 1. McMillan normalized density of states in the S side of an aluminum-tin proximity sandwich at fixed values of the potentials Δ_S^{ph} = 1.0 meV, Δ_N^{ph} = 0.1 meV, and $B_N = B_S = 2$, $v_{FN} = v_{FS} = 10^8$ cm sec^{-1}. Also d_S = 75 Å for all curves; d_N = 7.5 Å for curve a, d_N = 75 Å for b and d, d_N = 750 Å for c, e, and g, and d_N = 7500 Å for f and h. $\alpha = 0.002$ for a, b, and c; $\alpha = 0.02$ for d, e, and f; and $\alpha = 0.2$ for g and h. At a given value of α the shape of the peak structure is almost insensitive to the actual thickness of the films. For clarity the origin $N_S = 0$ is displaced for different curves.

α and for fixed values $\Delta_S^{ph} = 1$ meV, $\Delta_N^{ph} = 0.1$ meV.

The various parameters in each film are correlated by the equations[1]

$$\Gamma_N = \frac{\hbar v_{FN} \alpha}{4 B_N d_N} \text{ and } \Gamma_S = \frac{\hbar v_{FS} \alpha}{4 B_S d_S} , \quad (1)$$

where v_F is the Fermi velocity and B is a function of the mean free path and thickness. For extremely weak coupling (curves a, b, and c), the peak $P2$ in the density of states is sharp and peak $P1$ is very small. When the coupling is increased (larger α), the peak $P2$ becomes broader, while $P1$ grows in magnitude. For strong coupling (curves g and h), $P2$ disappears and $P1$ alone remains, but its magnitude is relatively small.

The temperature variation of the peak positions and of the potentials Δ_S^{ph} and Δ_N^{ph} can be calculated from the self-consistent conditions [Eq. (2) of Ref. 1]. For aluminum and tin, the bulk values $\lambda_N = 0.171$, $\omega_c^N = 32.21$ meV, $\lambda_S = 0.246$, and $\omega_c^S = 16.78$ meV were used; also $\Gamma_S/\Gamma_N = 5.0$, $B_N = B_S = 2$, $v_{FN} = v_{FS} = 1 \times 10^8$ cm/sec; and the values d_N = 750 Å, and $\alpha = 0.001$, 0.01, and 0.1 were chosen for the computations. It can be seen from Fig. 2 that for weak coupling between the films (case a), the higher-energy peak $P2a \simeq \Delta_{S,a}^{ph}$ follows closely the BCS temperature variation of the tin gap, while the lower-energy peak $P1a \simeq \Delta_{N,a}^{ph}$ follows the BCS temperature depen-

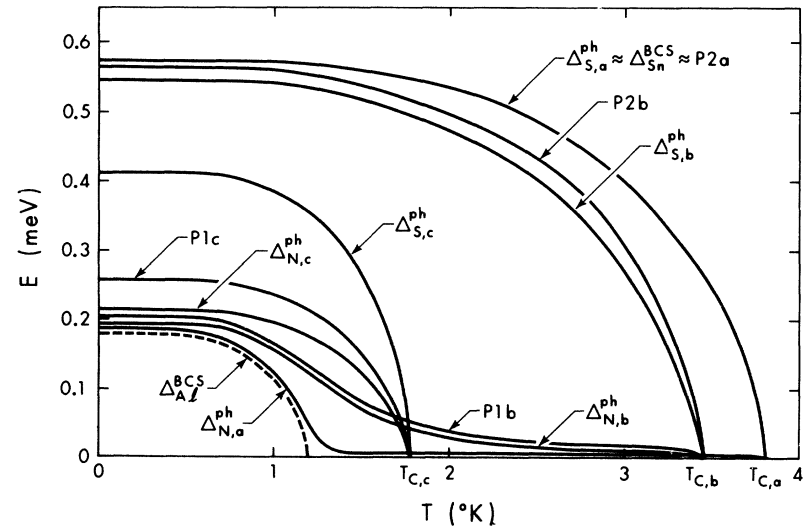

FIG. 2. Temperature variation of the peaks $P1$ and $P2$ in the density of states in the tin side of an aluminum-tin proximity sandwich and the potentials Δ_S^{ph} and Δ_N^{ph} when $d_N > d_S$. Bulk values $\omega_c^N = 32.21$ meV, $\lambda_N = 0.171$ were used for aluminum; $\omega_c^S = 16.78$ meV, $\lambda_S = 0.246$ for tin. $\Gamma_S/\Gamma_N = 5$ for all curves, $\Gamma_S = 0.005$ meV for a, $\Gamma_S = 0.05$ meV for b, and $\Gamma_S = 0.5$ meV for c. BCS variation of the tin gap is indistinguishable from Δ_{Sa}^{ph}. $T_c = 3.80$ °K for a, $T_c = 3.42$ °K for b, and $T_c = 1.78$ °K for c. The dashed curve represents BCS variation of the aluminum gap.

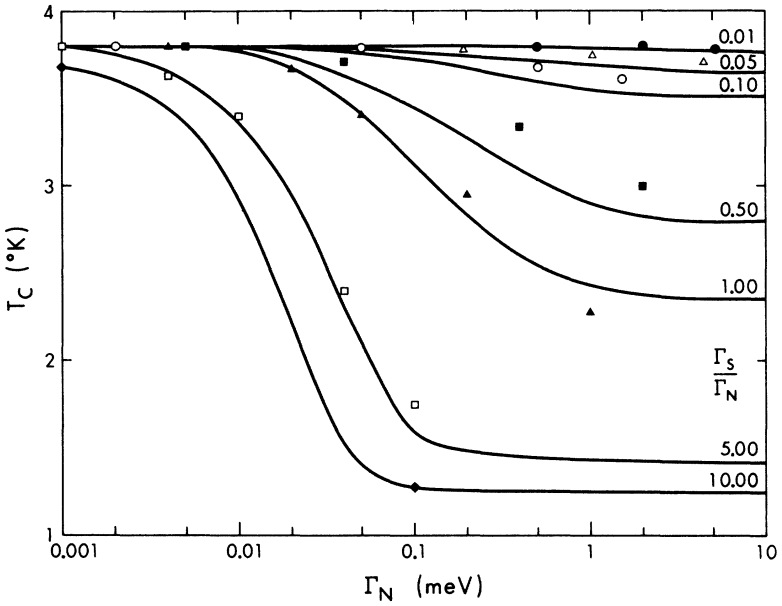

FIG. 3. Critical temperature T_c of an aluminum-tin proximity sandwich versus Γ_N. The parameter is Γ_S/Γ_N. The solid curve represents direct calculation. ■, ▲, □, ◇: estimate from plots similar to Fig. 2; ●, △, ○: estimate using BCS approximation. For further identification of the symbols see Fig. 4.

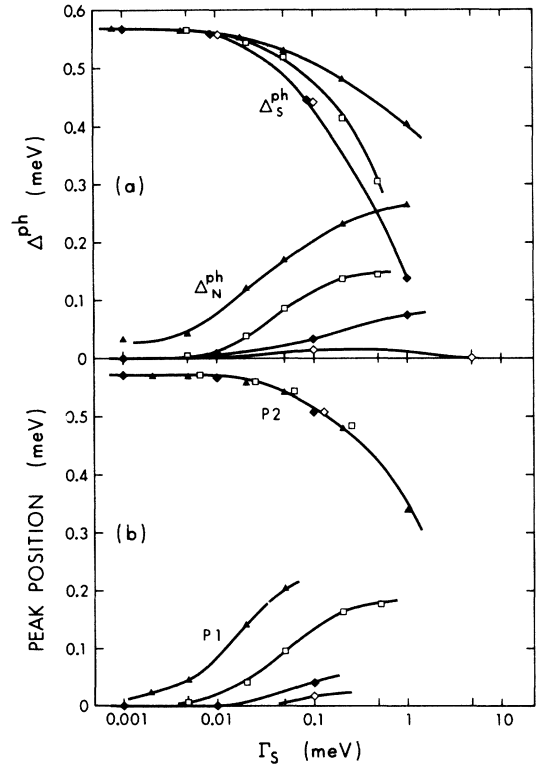

FIG. 4. Self-consistent calculations of the McMillan model for an aluminum-tin sandwich when $d_N > d_S$. (a) Values of potentials Δ^{ph}_S and Δ^{ph}_N as a function of Γ_S at 1.4 °K. (b) Peak positions in the S side as a function of Γ_S at 1.4 °K. ▲, $\Gamma_S/\Gamma_N = 1$, □, $\Gamma_S/\Gamma_N = 5$, ♦, $\Gamma_S/\Gamma_N = 10$, and ◇, $\Gamma_S/\Gamma_N = 50$.

dence for the aluminum gap at low temperatures, but deviates progressively as the temperature is raised, and only approaches zero at T_c of the overall sandwich. For strong coupling (case c), the peaks are no longer separated.

Also, as the coupling is increased, in contrast to the case $d_N < d_S$ (see Ref. 1), the critical temperature of the proximity sandwich is markedly reduced. The critical temperature of proximity sandwiches according to the McMillan model may be obtained from the intersection of the Δ^{ph}_S or $P2$ curves in Fig. 2 with the zero-energy axis. However, this method is not too reliable because the computer calculation converges slowly in this region. A procedure for direct calculation of T_c from the McMillan equations is described in the Appendix.[4] In Fig. 3, the critical temperature T_c of proximity sandwiches is plotted as a function of Γ_N. The solid lines are calculated using the direct method; the various symbols show the values of T_c estimated from extrapolation of curves similar to Fig. 2. Taking into account the inaccuracy of extrapolation, the agreement is quite satisfactory. For $\Gamma_S/\Gamma_N < 0.5$, the critical temperature calculated using the direct method also agrees within 2% with the critical temperature estimated using the BCS relation

$$2\Delta^{ph}_S(T=0)/kT_c \simeq 3.5.$$

In Fig. 4, the self-consistent values of Δ^{ph}_S and Δ^{ph}_N and of the peak positions at 1.4 °K are plotted against Γ_S for different ratios of Γ_S/Γ_N. The values of Δ^{ph}_N and the position of peak $P2$ are almost independent of Γ_N (and therefore of B_N or d_N) over a wide range of Γ_S. The values of Δ^{ph}_N and peak $P1$ are slightly dependent on Γ_N. However, if Δ^{ph}_S and Δ^{ph}_N or the peak positions

were plotted versus Γ_N for different ratios of Γ_S/Γ_N, the much stronger dependence of these properties on Γ_S would be emphasized. This is to be contrasted with the strong dependence of these properties on Γ_N and weak dependence on Γ_S in the N side of the sandwich (see Fig. 3 of Ref. 1).

The region in which the double peak may be experimentally observed from the tin (S) side is estimated to be

$$0.001 \lesssim \Gamma_S \lesssim 1.0 \text{ meV}. \quad (2)$$

The lower limit is determined by the magnitude of $P1$, which becomes smaller as Γ_S is decreased, while the upper limit is approximately the point where the two peaks merge, as may be determined from Fig. 4(b). Using Eq. (1) with $v_{FS} = 10^8$ cm/sec and $B_S = 2$, Eq. (2) becomes

$$10^{-6} \lesssim \alpha/d_S \lesssim 10^{-3},$$

where d_S is expressed in Å. The range of α and of Γ_S/Γ_N over which the double peak may be observed is greater in the S side than in the N side of the proximity sandwich.

EXPERIMENTS

The experimental procedures have already been described in Ref. 1. The only change for the experiments described here was in the preparation of the decoupling barrier between the metals in proximity. Because tin oxidizes more slowly than aluminum does, higher pressures (up to 0.2 Torr) and longer oxidation times (up to 1000 sec) were used in order to produce the desired values of α.

We have also attempted to control α by oxidation of the tin in a glow discharge or by evaporation of a thin layer of SiO on its surface before the aluminum was deposited. The glow-discharge-assisted oxidation was carried out for 60 sec in an atmosphere of dry oxygen at a pressure of 0.2 Torr with a glow current of 1 mA. This procedure produced a thick oxide (extremely small α), so that the double peak in the McMillan density of states could not be resolved. Although, in the experiments with SiO, the layers of average thickness from 4 to 18 Å were evaporated from a distance of about 45 cm, the results were those that might be expected for a very nonuniform decoupling barrier, and therefore we infer that SiO is not suitable for this purpose.

TUNNELING INTO S SIDE OF PROXIMITY SANDWICH

The experimental tunneling conductance is compared with the calculated conductance using the tunneling integral and the density of states for the aluminum electrode B as described in Ref. 1 [Eq. (8)].

Tunneling from Normal-State Metal

In contrast to tunneling into the N side of a proximity sandwich, tunneling from a normal-state metal into the S side of a sandwich does not offer any information that will aid in the identification of the parameters of the proximity sandwich. The dependence[5] of $1 - \sigma(0)$ on $1 - T/T_c$ calculated for the McMillan model is very close to the BCS dependence. This result is to be expected because in the S side of the proximity sandwich the peak $P2$ in the density of states is dominant. For all α, the temperature dependence of this peak, shown in Fig. 3, resembles the temperature dependence of the gap in a BCS superconductor, and therefore the behavior of the proximity sandwich must be BCS-like.

The experimental observations agree quite well with the theoretical predictions. A plot of the experimental dependence for three junctions with different α is presented in Fig. 5. The slopes are very close to unity but in some cases the lines are shifted toward smaller values of $1 - \sigma(0)$. The largest shift was observed for junction $Q30$ shown in Fig. 5. The shift could be caused by a background conductance (zero bias anomaly) that varies with temperature, or by variation of α over the sample area, or by a combination of both effects. A variation of α could affect the plot in the following way: The measured critical temperature T_c will correspond to the part of the junction with the

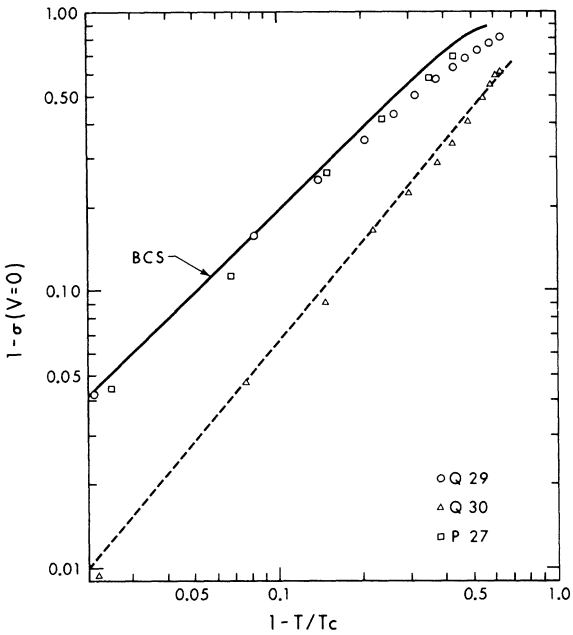

FIG. 5. Experimental dependence of $1 - \sigma(V=0)$ on $1 - T/T_c$. $\sigma(V=0)$ is the normalized tunneling conductance at zero bias between a normal-state metal and the S side of an aluminum-tin proximity structure.

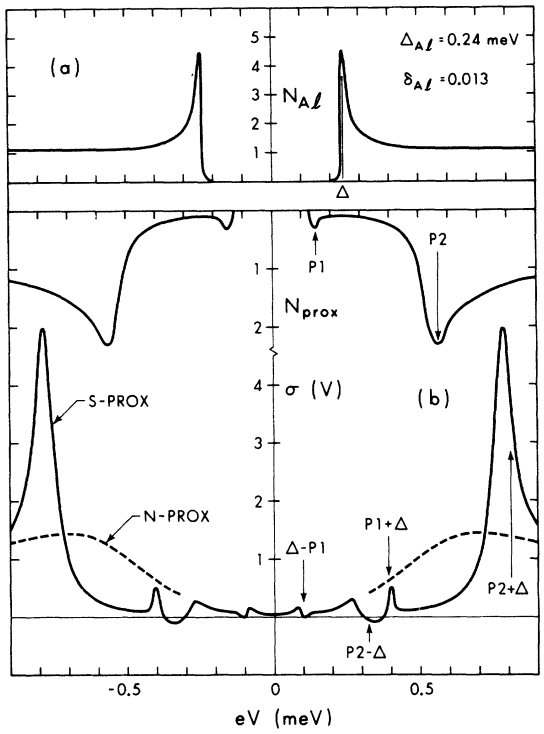

FIG. 6. Illustration of the occurrence of multiple peak structure in the tunneling conductance between an ordinary superconductor and the S side of an aluminum-tin proximity sandwich. (a) Normalized density of states in the superconducting aluminum, N_{Al} (characterized by $\Delta_{Al} = 0.24$ meV, $\delta_{Al} = 0.013$), and proximity sandwich, N_{prox} (characterized by $\Gamma_S = 0.05$ meV, $\Gamma_N = 0.01$ meV, $\Delta_S^{ph} = 0.539$ meV, and $\Delta_N^{ph} = 0.141$ meV). When voltage is applied the densities of states shift on the energy scale. (b) Resulting calculated tunneling conductance at 1.1 °K is shown by the solid line. Expected structures at $P1 \pm \Delta$ and $P2 \pm \Delta$ are indicated by arrows. For comparison, the tunneling conductance between a normal-state metal and the same proximity sandwich at the same temperature is shown by the dashed line.

smaller α and therefore $1 - T/T_c$ will have a high value, while $\sigma(0)$ will be equal to that for the majority of the junction area.

Tunneling from Superconductor

The normalized conductance for tunneling from a superconductor into the S side of a weakly coupled proximity sandwich exhibits the multiple-peaked structure shown in Fig. 6(b). The curve was constructed for tunneling at 1.1 °K between the density of states for aluminum and the McMillan density of states shown in Fig. 6(a). The expected positions of the structure are indicated by arrows at $P1 \pm \Delta$ and $P2 \pm \Delta$. One can see very poor coincidence between the expected energy of the structure and actual energy of the peak maxima. Also, in certain cases, a peak appears in the normalized tunneling conductance associated with a dip in the McMillan density of states so that extra peaks sometimes appear. These effects make final interpretation of the tunneling conductance curves quite difficult.

In Fig. 7, an experimental curve at 1.4 °K for junction $O22$ is compared with a calculated curve using $\Gamma_S = 0.03$ meV and $\Gamma_N = 0.012$ meV. The value for Γ_S was found by fitting the peak position to Fig. 4 and Γ_N was found from the condition $\Gamma_S/\Gamma_N = d_N/d_S$, obtained by assuming $B_N = B_S$ and $v_{FN} = v_{FS}$. The peak positions agree quite well, but the structure on the calculated curve is sharper than the experimental structure. However, the experimental curve may be a combination of different McMillan curves, such as would be obtained if the transmission probability α was not constant over the area of the junction. A double-peaked structure in the density of states on the S side of a Cu-Pb proximity sandwich has also been observed by Freake and Adkins[6] in a tunneling experiment from a normal-state metal at $T = 0.06$ °K, but a quantitative correlation to the parameters of the McMillan model was not attempted.

The temperature dependence of $P1 \pm \Delta$ and $P2 \pm \Delta$ should arise from the combination of the tempera-

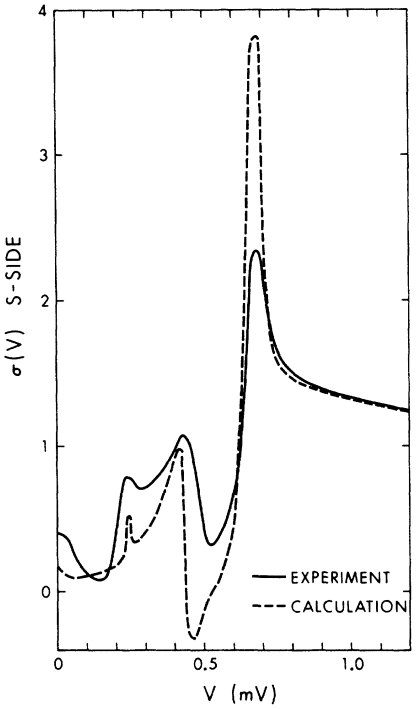

FIG. 7. Comparison of experimental and theoretical normalized conductance for tunneling from superconducting aluminum into the S side of aluminum-tin proximity sandwich. Solid line: experiment $O22$, $T = 1.4$ °K, $d_{Al} = 2790$ Å, $d_{Sn} = 1015$ Å; dashed line: calculated with $\Gamma_S = 0.03$ meV, $\Gamma_N = 0.012$ meV, $\Delta_S^{ph} = 0.55$ meV, $\Delta_N^{ph} = 0.10$ meV. Aluminum electrode from which the tunneling was done is characterized by $\Delta_{Al} = 0.12$ meV, and $\delta = 0.013$.

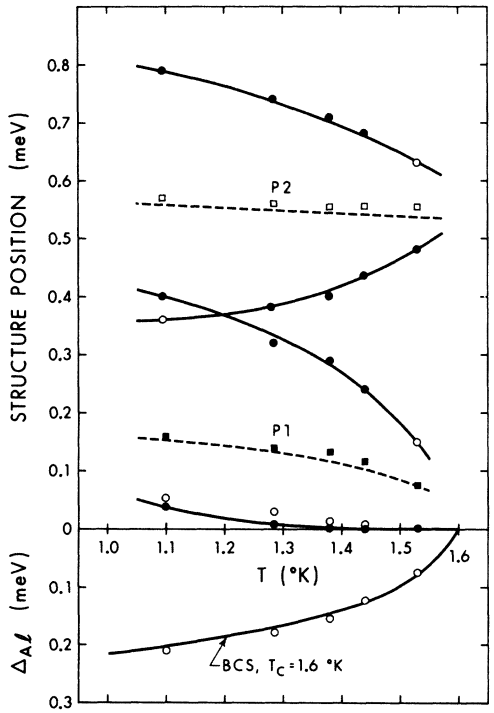

FIG. 8. Experimental temperature dependence of the peak positions. ●: experimental points corresponding to $\Delta - P1$, $P1 + \Delta$, $P2 - \Delta$, and $P2 + \Delta$, junction $O22$; ○: calculated values using the experimental points (note the consistency of the results for $\Delta - P1$); ■: $P1$, □: $P2$, positions calculated from experimental points. In the lower graph the gap of the aluminum electrode from which tunneling into the proximity structure was performed is shown (○) as calculated from the experimental points in the upper part. For comparison the solid line shows the BCS temperature variation of a gap with $T_c = 1.6\,°K$.

tures and reconstruct the position of the fourth, or check the consistency of the method where all four structures are resolved. The values of $P1$ and $P2$ calculated from the experimental values of $P1 \pm \Delta$ and $P2 \pm \Delta$ are compared with the theoretical values (dashed line). Also Δ, the gap of the aluminum electrode, can be compared with the temperature variation of a BCS gap with $T_c = 1.6\,°K$, as has been done in the lower part of Fig. 8. Remarkably good agreement is obtained.

Dependence of Data on α

In Tables I and II, the Γ_S values determined from the experimental data, and the transmission probabilities α calculated from them, are presented. The Γ values were determined by two different methods: first by comparison of the experimental critical temperature T_c with Fig. 3, and second by comparison of the experimental values of peak positions with Fig. 4. The α values were determined using Eq. (1) and putting $B_S = 2$.

The results for the junctions in which the transmission probability α was controlled by different amounts of thermal oxidation of the tin layer are presented in Table I. It is clear that α decreases systematically as the amount of oxidation at the interface increases, being in about the ratio 200 : 30 : 1 for the samples of Secs. I, II, and III, respectively, of Table I. This range of α values was achieved by creating the following conditions during the time interval Δt between the evaporation of tin and aluminum: Sec. I: pressure ~ 5×10^{-7} Torr, $\Delta t \simeq 60$ sec; Sec. II: pressure ~ 0.2 Torr of oxygen dried in a liquid-nitrogen trap, $\Delta t \simeq 100$ sec; and Sec. III: pressure ~ 0.2 Torr of dry oxygen, $\Delta t \simeq 1000$ sec. When Sec. I of Table I is compared with Sec.

TABLE I. Transmission probability α and Γ_S as a function of the oxidation conditions for Sn-Al proximity sandwiches. Peaks P1 and P2 are measured at 1.4 °K, unless otherwise stated.

Section	Junction[a]	d_S (Å)	d_N (Å)	$\frac{\Gamma_S}{\Gamma_N} = \frac{d_N}{d_S}$	Critical temperature T_c T_c (°K)	Γ_s (meV)	α ($B=2$)	Peak positions $P1$ and $P2$ $P1$ (meV)	$P2$ (meV)	Γ_s (meV)	α ($B=2$)
	$M17$	457	2405	5.27	2.16	0.26	0.15	0.31		0.7	0.40
	$N19$	688	2200	3.20	1.90	0.35	0.30	0.30		0.6	0.52
I	$O21$	822	1679	2.04	2.19	0.41	0.42	0.25		0.4	0.41
	$P27$	578	1176	2.03	2.35	0.26	0.19	0.39[b]		0.9	0.65
	$P28$	918	1053	1.15	2.59	0.35	0.39	0.35[b]		0.6	0.69
II	$O22$	1015	2790	2.75	3.49	0.036	0.045	0.09	0.56	0.04	0.050
	$Q30$	617	767	1.24	3.42	0.043	0.035	0.22[b]	0.56[b]	0.04	0.031
	$R32$	995	1105	1.11	3.10	0.060	0.049				
III	$Q29$	575	732	1.27	3.76	<0.0073	<0.01	0.11[b]	0.60[b]	0.002	0.0014
	$R31$	532	680	1.28	3.76	<0.0070	<0.01	~0.02	0.58	0.001	0.0008

[a]Junctions designated by the same letter were prepared at the same time on the same substrate.

[b]These values were measured at 1.1 °K.

TABLE II. Transmission probability α for barriers formed by the evaporation of SiO or glow-discharge oxidation. Peaks $P1$ and $P2$ were measured at 1.4 °K.

Junction[a]	Formation of α	d_S (Å)	d_N (Å)	$\frac{\Gamma_S}{\Gamma_N}=\frac{d_N}{d_S}$	Critical temperature T_c			Peak positions $P1$ and $P2$			
					T_c (°K)	Γ_S (meV)	α ($B_S=2$)	$P1$ (meV)	$P2$ (meV)	Γ_S (meV)	α ($B_S=2$)
$K12$	4 Å SiO	992	1680	1.69	3.49	0.034	0.042	0.158	0.458	0.30	0.57
$K11$	8 Å SiO	470	1620	3.44	3.67	0.021	0.012	0.158	0.481	0.20	0.12
$L13$	12 Å SiO	536	1673	3.12	3.70	0.013	0.0084	0.09	0.60	0.05	0.034
$L14$	18 Å SiO	970	1731	1.79	3.79	<0.0054	<0.0065	0.08	0.585	0.04	0.049
$I4$	Glow Discharge[b]	1015	56	0.055					0.61	<0.05	<0.0063
$J6$	Glow Discharge[b]	630	920	1.46					0.62	<0.05	<0.0039

[a]Junctions designated by the same letter were prepared at the same time on the same substrate.

[b]The glow-discharge current was 1 mA for 60 sec in 0.15 Torr of dry O_2.

II of Table I of Ref. 1, in which the oxidation conditions are about the same, one can immediately see that the α value obtained by the oxidation of aluminum is much smaller than that obtained by oxidation of tin, which is to be expected because aluminum oxidizes more readily than does tin.

The α values derived from the critical temperature are smaller than those derived from the peak positions. The difference may arise from slight nonuniformity of the oxide layer which forms the barrier between the films in proximity. Regions with thicker oxide will have a smaller value of α and a higher value of T_c. In the experiments we will detect the highest T_c in the sample, thus obtaining a smaller value of α than the average value which is measured by the peak positions. The discrepancy between the α values determined by the two methods is most remarkable in Sec. I. This probably arises from the fact that the McMillan model is valid only for $\alpha \ll 1$, while the values of α in this section range from 0.15 to 0.70.

We have also attempted to control α by other means. The results of these experiments are collected in Table II. A thin layer of SiO was evaporated in between the aluminum and tin in junctions K and L. The thickness of SiO was calculated from the density $\rho = 2.165$ g/cm^3 and known mass sensitivity of the frequency of the quartz-crystal thickness monitor. The sandwiches produced in this way usually exhibited more peaks in the conductance curve than predicted by the McMillan model. When the peaks were plotted against temperature, it looked as if peaks from different junctions were drawn onto the same sheet of paper. We attributed this behavior to the inhomogeneity of the SiO layer, which probably condenses in islands. The resulting effect is equivalent to two junctions in parallel, one with a high value of α and the other one with a small value of α. Also a very large discrepancy between α determined from T_c and from the peak positions (the strongest peaks were chosen) speaks for a large variation of α. The glow-discharge method was employed to control the value of α in junctions I and J. The method produced very thick oxide and resulted in very weak coupling between the films.

CONCLUSION

The tunneling characteristics of junctions between aluminum base layers and the tin side of proximity sandwiches formed by evaporated films of aluminum and tin have been measured. The coupling of the proximity films has been limited by allowing slight oxidation at the interface. The transmission probability of the oxidized interface was related both to the critical temperature of the sandwich and to the peak positions in the McMillan density of states.

When the aluminum base layer was superconducting, a multipeaked conductance curve was observed. The position of the peaks and their variation with temperature, as well as their dependence on the proximity film coupling, have all been compared with the McMillan theory with good agreement. The McMillan theory predicts sharper peaks than are observed, which probably arises, at least partly, from lack of uniformity of the decoupling barrier in the specimens.

Taken together with earlier results from tunneling experiments into the aluminum side of similar proximity sandwiches, these investigations demonstrate that the McMillan model of the proximity effect describes the tunneling properties of aluminum-tin evaporated films very well.
ture dependence of the McMillan peak structure (see Fig. 2) and the BCS temperature dependence of the gap edge in the aluminum electrode. The results of a typical experiment are plotted in Fig. 8. Since there are four structures and only three unknowns, $P1$, $P2$, and Δ, it is possible to calculate the unknowns at each temperature from three struc-

ACKNOWLEDGMENTS

We are grateful to Dr. J. G. Adler and Dr. J. S. Rogers for many helpful discussions. We also wish to thank H. McClung for technical assistance. We are particularly indebted to R. Teshima for help with the mathematical problems that arose in the computer calculations.

APPENDIX: CALCULATION OF CRITICAL TEMPERATURE OF McMILLAN MODEL

The method utilizes the fact that Δ_S^{ph} goes to zero when T goes to T_c.

First, new variables x, y, and γ are defined by

$$\Delta_S = x\,\Delta_S^{ph}, \quad \Delta_N = y\,\Delta_N^{ph}, \quad \Delta_N^{ph} = \gamma\,\Delta_S^{ph}. \tag{A1}$$

The new variables are introduced into Eqs. (1) and (2) of Ref. 1 and the equations are calculated in the limit $\Delta_S^{ph} \to 0$, giving

$$\begin{aligned} x\left(1+\frac{i\Gamma_S}{E}\right) - y\frac{i\Gamma_S}{E} &= 1, \\ x\frac{i\Gamma_N}{E} - y\left(1+\frac{i\Gamma_N}{E}\right) &= -\gamma \end{aligned} \tag{A2}$$

and

$$\gamma = \lambda_N \int_0^{\omega_c^N} \mathrm{Re}\left(\frac{y}{E}\right) \tanh\frac{E}{2T}\,dE,$$

$$1 = \lambda_S \int_0^{\omega_c^S} \mathrm{Re}\left(\frac{x}{E}\right) \tanh\frac{E}{2T}\,dE. \tag{A3}$$

Equations (A2) can be solved for x and y and the results put into Eqs. (A3). When eliminating γ from Eqs. (A3), after substitution of x and y, we get

$$F \equiv \frac{\lambda_N\lambda_S\Gamma_N\Gamma_S I_1 I_3}{1-\lambda_N I_2/(\Gamma_S+\Gamma_N) - \lambda_N\Gamma_S I_1} + \frac{\lambda_S I_4}{\Gamma_S+\Gamma_N} + \lambda_S\Gamma_N I_3 - 1 = 0, \tag{A4}$$

where

$$I_1 = \int_0^{\omega_c^N} D(E)\,dE, \quad I_2 = \int_0^{\omega_c^N} E^2\,D(E)\,dE,$$

$$I_3 = \int_0^{\omega_c^S} D(E)\,dE, \quad I_4 = \int_0^{\omega_c^S} E^2\,D(E)\,dE,$$

and

$$D(E) = \frac{\Gamma_N+\Gamma_S}{E^2+(\Gamma_N+\Gamma_S)^2}\ \frac{1}{E}\tanh\frac{E}{2T}.$$

The temperature for which $F = 0$ is the critical temperature of the McMillan model. This equation has more than one root, but the one of physical interest lies in the temperature interval between 1.2 and 3.8 °K.

---

*Research supported in part by the National Research Council of Canada.

[1]J. Vrba and S. B. Woods, Phys. Rev. B 3, 2243 (1971).

[2]J. Vrba and S. B. Woods, in *Proceedings of the Twelfth International Conference on Low-Temperature Physics*, edited by E. Kanda (Academic Press of Japan, Tokyo, 1971).

[3]W. L. McMillan, Phys. Rev. 175, 537 (1968).

[4]We are grateful to R. Teshima for developing the mathematical method used here.

[5]E. Guyon, A. Martinet, S. Mauro, and F. Meunier, Physik Kondensierten Materie 3, 123 (1966).

[6]S. M. Freake and C. J. Adkins, Phys. Letters 29A, 382 (1969).

PHYSICAL REVIEW B VOLUME 4, NUMBER 1 1 JULY 1971

Exchange Energy of an Electron Gas in a Magnetic Field

R. W. Danz and M. L. Glasser
Battelle Memorial Institute, Columbus, Ohio 43201

(Received 16 February 1971)

The exchange energy of an electron gas is calculated in the zero-temperature limit. In high magnetic fields, it is shown that the exchange energy dominates the independent-particle energy, but in low and intermediate fields becomes much less important. Modifications due to band structure and application to the de Haas–van Alphen effect are discussed briefly.

I. INTRODUCTION

The free energy of a dense electron gas, which forms a basis for studying the thermodynamic properties of metals, is assumed to have a convergent expression in powers of the parameter describing the electron-electron Coulomb interaction. (This parameter is customarily related to the mean interelectron spacing r_s.) The leading